DOE/ER/60894--7

SPECT ASSAY OF RADIOLABELED MONOCLONAL ANTIBODIES

FINAL PERFORMANCE REPORT:

MARCH 1992 - NOVEMBER 1995

Ronald J. Jaszczak, Ph.D.

Radiology Department

Duke University Medical Center

Durham, North Carolina 27710

DECEMBER 1995

PREPARED FOR THE U.S. DEPARTMENT OF ENERGY
UNDER GRANT NUMBER DE-FG05-89ER60894

1. PROGRESS REPORT

1.1. INTRODUCTION

Since the grant was last submitted for competitive renewal (March 1, 1992), this grant has fully or mainly supported 17 peer-reviewed manuscripts (Section 1.3.1). One United States Patent was issued that was fully supported by this grant (Section 1.3.2). There were 42 directly related peer-reviewed manuscripts for which this grant provided partial support (Section 1.3.3). In terms of book chapters and conference proceedings, there were 9 supported fully or mainly by this grant (Section 1.3.4) and 22 directly related and supported in part by this grant (Section 1.3.5). During the past project period, this grant has supported fully, or in part, 44 abstracts.

1.1.1. Original Specific Aims from March 1992 application

1. To develop and evaluate new filtered backprojection (FBP) and iterative reconstruction algorithms (Maximum Likelihood and Bayesian) for SPECT MAb imaging which are computationally fast and compensate for physical factors affecting SPECT data acquisition.
2. To evaluate *in vivo* SPECT quantification of indium-111-labeled MAb patient scans by comparing SPECT measurements with post-surgical assays of tissue biopsies.
3. To determine quantitative accuracy of SPECT and PET to measure I-123 and I-124 activities, respectively, in phantoms and in spontaneous tumors using radiolabeled MAbs.
4. To investigate potential utility of SPECT using pinhole collimation to image and quantify At-211 and I-131-radiolabeled therapeutic MAbs.

In the last renewal application (1992), support was requested for a period of 5 years at an average funding level of $204,500./year (average direct cost), or a total direct cost of about $1,022,500. The project was recommended for approval for 3 years at a level of $169,000./year (average direct cost), with a total funding level for 3 years of $745,000. (direct plus indirect cost). Through subsequent negotiations with DOE, the actual funds awarded were reduced to about $150,000./year (average direct cost), with a total funding level of $676,100. (direct plus indirect cost) for the 3 years.

Because of the reduced project period and reduced level of actual support awarded (i.e., greater than 33% reduction in direct costs and 40% in effort), it was necessary to narrow the overall scope of the project and prioritize the specific aims. We elected to defer extensive investigations of SPECT quantification of I-131-labeled MAbs until the next project period. The I-124 studies have been delayed since the design and fabrication of a appropriate cyclotron target for I-124 production has only recently been completed. Initial I-124 comparisons with I-123 are planned for the latter part of this year. We have concentrated our resources and effort on 1) developing and evaluating quantitative reconstruction algorithms with improved compensations for attenuation, scatter and geometric collimator response, 2) evaluating SPECT quantification of I-123 (a radionuclide appropriate for radioimmunodiagnosis) and At-211 (a radionuclide appropriate for radioimmunotherapy), and 3) developing and evaluating SPECT pinhole imaging for low and medium energy photons, such as those emitted by Tc-99m, I-123, and In-111. We believe we have made substantial progress towards these more focused specific objectives during the current project period.

1.1.2. Summary of Progress During Current Project Period

Since the project was last competitively reviewed we have made the following progress directed towards the 1992 Specific Aims.

1. Development and evaluation of quantitative reconstruction methods for SPECT imaging of radiolabeled MAbs
   - A. Development of 3D iterative reconstruction methods [2,8]
   - B. Development of new filtered backprojection reconstruction methods [12,16]
   - C. Development of improved TCT acquisition for nonuniform attenuation compensation [5,6,15,17, 18 [United States Patent Number 5289008]]
2. Determining the accuracy of SPECT to quantify I-123 and At-211 activities and biodistributions.
   - A. SPECT quantification of I-123 distribution [9,12,13]
   - B. Development of image registration methods [1,4,10]
   - C. SPECT quantification of At-211 distribution [3,11]
3. Investigate SPECT imaging of radiolabeled therapeutic MAbs using pinhole collimation.
   - A. Ultra-High Resolution, Small Field-of-View (FOV) Pinhole SPECT Imaging [7]
   - B. Pinhole SPECT Imaging of In-111 [14]

1.2. DESCRIPTION OF RESEARCH DURING CURRENT PROJECT PERIOD

1.2.1 Development and evaluation of quantitative reconstruction methods for SPECT imaging of radiolabeled MAbs

This area of our research has seen progress along three lines: (1) three-dimensional iterative reconstruction methods, (2) new filtered backprojection reconstruction methods, and (3) improved transmission computed tomography (TCT) acquisition for nonuniform attenuation compensation.

Development of three-dimensional (3D) iterative reconstruction methods. The objective of our initial work in this area [2] was to develop and evaluate an iterative reconstruction algorithm for SPECT that models in 3D the effects of uniform attenuation and detector response. The algorithm was 3D in the sense that it modeled both in-plane and cross-plane effects. The model was incorporated within the ML-EM reconstruction method and was compared with the filtered backprojection method (FBP) with Metz filter and Chang attenuation compensation in terms of quantitative accuracy and image noise. The methods were tested on Monte Carlo simulated data of the 3D Hoffman brain phantom. The simulation incorporated the effects of attenuation and distance-dependent detector response. Bias and standard deviation of reconstructed voxel intensities were measured in the gray and white matter regions. The results with the 3D iterative method showed that in both the gray and white matter regions as the number of iterations increased, bias decreased and standard deviation increased (Fig. 4 in [2]). Similar results were observed with FBP as the Metz filter power increased. In both regions, the iterative method had smaller standard deviation than FBP for a given bias. Reconstruction times for the ML-EM method were greatly reduced through efficient coding, limiting the source support region, and by computing attenuation factors only along rays perpendicular to the detector.

Subsequent to this work, refinements were made in the 3D iterative reconstruction algorithm that allowed more accurate physical modeling as well as greater computational efficiency [8]. The refinements included the incorporation of non-uniform attenuation modeling based on reconstructed transmission computed tomography (TCT) data. Also aiding in the efficiency and overall accuracy of the model was a technique termed region dependent reconstruction (RDR). With RDR, the FBP method is used to reconstruct areas of the image of minimal clinical importance, and the result is used to supplement the iterative reconstruction of the clinically important areas of the image. The 3D iterative reconstruction method was tested in three experimental phantom studies, a point source (a uniform cylinder, and an anthropomorphic thorax) and a patient Tc-99m labeled Sestamibi cardiac perfusion study. The point source data demonstrated the improvement in resolution with iteration (Fig. 3 in [8]). Images of the uniform cylinder allowed investigation of the edge and noise artifacts inherent in the algorithm (Figs. 4 and 5 in [8]). It was demonstrated with the patient data that the RDR technique produces essentially the ML-EM estimate in the cardiac region with substantial computational time savings (Figs. 11 and 12 in [8]).

We have recently developed an efficient 3D iterative reconstruction method that allows the incorporation of scatter into the reconstruction kernel in addition to detector response and attenuation. The inclusion of scatter effects in the kernel, or matrix, decreases the sparcity of the matrix and increases the program memory requirement if all non-zero matrix elements are to be retained in memory during program execution. For example, for a 64^3 image matrix and a 64^3 projection matrix, the fully 3D reconstruction matrix requires approximately 275 Gbytes of memory (assuming 4 bytes/element). If only 50% of this reconstruction matrix contains non-zero elements, the task is still impractical.

An approach that we have been investigating proposes that instead of storing all non-zero elements, store only those not "close to" zero. The essential innovation of this approach is that the "close to" zero cut-off threshold is determined independently for each image voxel, and for each image voxel the sum of its elements above the threshold value is a fixed percentage of the sum of all of its elements. This can be expressed as:

$$\frac{c_{ij}\ (\text{for } c_{ij} \geq T_j)}{\sum_i c_{ij}\ (\text{for all } i)} \times 100 = X\%$$

where c_{ij} is the kernel element for voxel j and projection bin i, T_j is the computed threshold value, and X% is the pre-determined threshold criterion. Note that i indexes projection bins over all projection angles. In implementing this approach, the reconstruction matrix is inspected before the first iteration to determine for each image voxel first T_j and then the extent of the projection space over which the matrix elements are equal or above threshold. Indices defining this supra-threshold region in the projection space are recorded for each voxel.

We have evaluated this approach to 3D iterative reconstruction using simulated phantom data. The phantom consisted of an 11.1 cm radius cylinder containing two spheres, both 1.7 cm in radius. One sphere contained water with no activity and the other contained activity in a 5:1 ratio with the activity in the remainder of the cylinder. Projection data were generated using a kernel that was obtained from analytical solutions to the photon transport equation for point sources in an attenuating medium (Riauka and Gortel 1994). Poisson noise was then added to the projection data after scaling the data to a maximum count per projection bin of 150. The data were reconstructed using the ML-EM algorithm and pre-determined threshold criteria including 100%, 98%, 90%, and 80%. In order to minimize the effect of inaccuracies in the reconstruction kernel, the same kernel that was used to generate the data was also used for the reconstruction. Although this is an unrealistic simplification, it does allow study of the effects due to the thresholding of the reconstruction kernel. The images and profiles from this study are shown in Figs. 1 and 2, respectively. The images have been displayed using the same gray scale mapping. The profile is oriented vertically in the images, is one voxel wide, and intersects the centers of the spheres. Note that as the threshold criterion is lowered, the absolute activity level increases, and the region of the cold sphere moves farther from zero intensity. Differences between the 100% and 98% images and profiles are difficult to visualize.

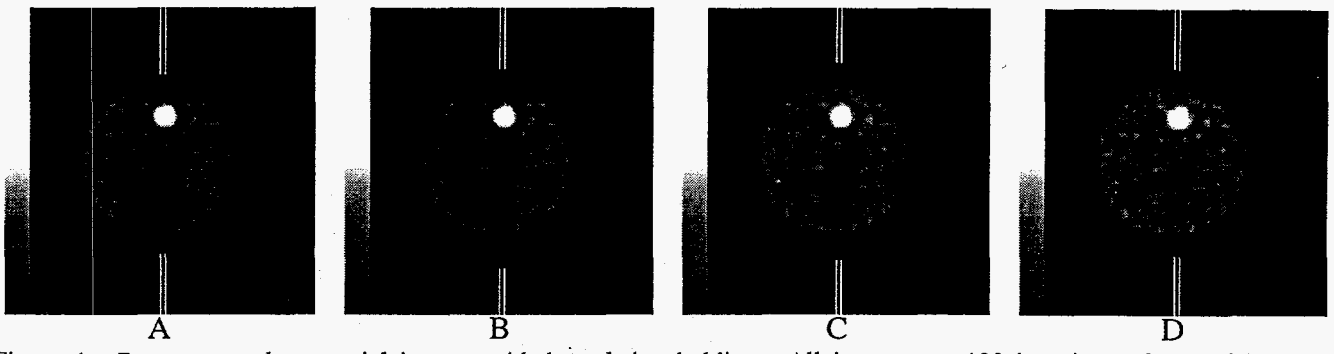

Figure 1. Reconstructed transaxial images with kernel thresholding. All images are 100 iterations of ML-EM. (A) 100% criterion, i.e. no thresholding, (B) 98%, (C) 90%, (D) 80%.

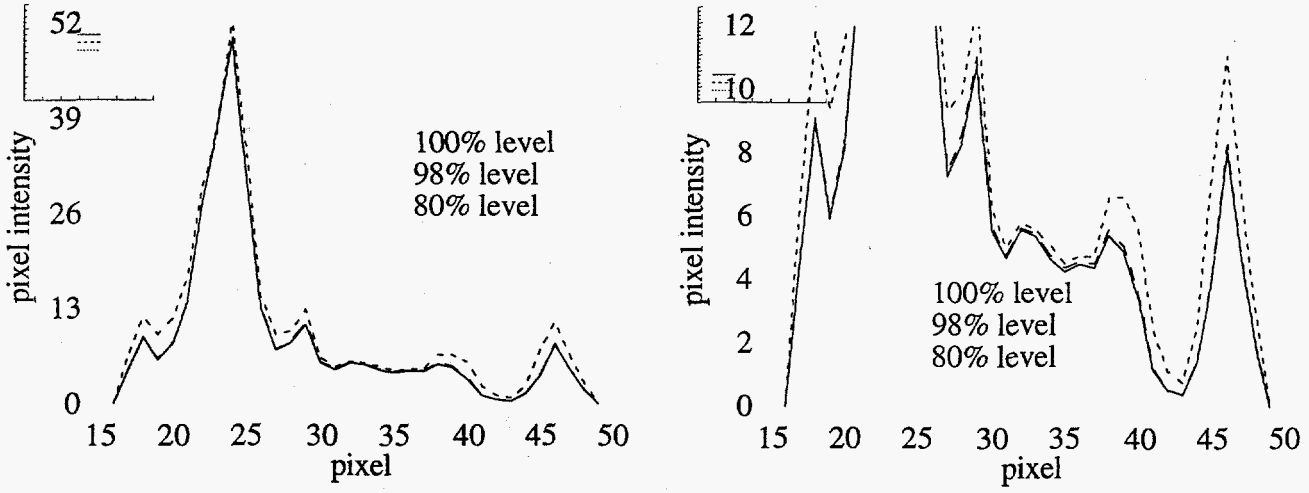

Figure 2. Profiles through images of Fig. 1. (left) full scale, (right) scaled to emphasize lower intensities. The 90% example has been omitted for ease of visualization.

Sphere contrast was measured in these images considering a range of iteration stopping points up to 200 iterations. Sphere contrast was defined as the absolute value of: (average sphere count density - average background count density)/(average background count density). The average sphere count density was obtained using an ROI equal to the known size of the sphere and at the known sphere location. The average background count density was obtained using a large ROI placed in the uniform background region. (While the true contrast should be measured in the absence of noise effects, the size of these ROI's likely minimizes noise effects.) The results are shown in Table 1 for the hot sphere and Table 2 for the cold sphere. One can see from these tables the decrease in contrast with decrease in the threshold criterion. However, the decrease in contrast from 100% to 98% is relatively small.

TABLE 1 Hot sphere contrast

	threshold criterion			
iteration	100%	98%	90%	80%
25	2.64	2.59	2.42	2.32
50	2.80	2.75	2.53	2.39
100	2.86	2.80	2.58	2.42
200	2.90	2.84	2.61	2.44

TABLE 2 Cold sphere contrast

	threshold criterion			
iteration	100%	98%	90%	80%
25	0.532	0.531	0.515	0.508
50	0.633	0.630	0.602	0.580
100	0.708	0.703	0.664	0.624
200	0.759	0.751	0.702	0.644

TABLE 3 Memory requirements (Mbytes) and processing times (seconds).

	threshold criterion			
	100%	98%	90%	80%
memory required	356†	465	99	34
time/iteration	1,065	32	7.5	6.0

†See text for explanation of the value 356 Mbytes.

The computer memory requirement and execution time per iteration (Digital Equipment Corp. Model 3000/800) are shown in Table 3. Note that because the 100% case required an impractical amount of memory (approximately 275 Gbytes), the entire reconstruction kernel could not be retained in program memory (~750 Mbytes) throughout execution. Instead, the kernel for one angle was retained in memory and kernel elements for all other angles were re-computed every iteration by interpolation. This is reflected in the decrease in memory requirement shown in Table 3 (356 Mbytes) for the 100% case. The large increase in execution time for the 100% case is due mainly to the larger reconstruction kernel and, to a lesser extent, the required interpolation. It is possible that a threshold of 90-95% may be acceptable for many imaging situations.

Development of new filtered backprojection reconstruction methods. A new method of FBP reconstruction that is applicable to converging geometry has recently been proposed [16]. The method is aimed at improving the noise characteristics in the reconstructed image by making more efficient use of the measured converging projection data. A conventional method of implementing FBP for converging beam geometries utilizes a "pixel driven" approach wherein the backprojection proceeds by successively stepping through a series of equally spaced grid points in the image space. The grid points are usually taken to represent the centers of an array of square pixels. The reconstructed value for each grid point is determined by summing backprojection contributions to the grid point from each angular view. The backprojection contribution for a given grid point at a given angular view is determined by mapping the grid point to the filtered projection space and appropriately interpolating a value of the filtered projection about the mapped grid point location. The interpolation is typically performed using a two or four bin linear scheme.

With converging beam geometries, however, this type of pixel driven approach using equal size image pixels and projection bins may not perform satisfactorily, in terms of image noise, when reconstructing data with limited counting statistics (e.g. typical SPECT data). This is because the relationship between image grid point spacing and projection bin spacing with convergent geometry is not constant due to magnification. In fact, adjacent grid points near the focal point will map to the projection space over a region of several projection bins (Fig. 2 in [16]). To overcome this limitation, we have proposed a pixel driven algorithm that effectively utilizes all projection data for every backprojection row by explicitly considering the effect of magnification on the mapping of adjacent grid points (pixels) to the projection space. The algorithm creates an "effective" projection bin whose size is position dependent. We have shown using a simulated phantom, experimental "Cold Rod" and line source phantoms, and patient data, that the new FBP algorithm which uses a position-dependent effective projection bin length can result in an improvement in image noise with very little resolution degradation compared with conventional pixel driven methods for fan beam data (Figs. 4-7 in [16]).

1.2.2. Development of improved TCT acquisition for nonuniform attenuation compensation

The objective of this work was to develop and evaluate a new acquisition system to obtain gamma transmission computed tomography (TCT) data for determining attenuation maps to compensate SPECT emission scans [5]. The system consists of a Tc-99m line source placed near the focal line of a 114 cm focal length fan beam collimator which is mounted on one detector of a triple-camera SPECT system (Fig. 1 in [5]). Surrounding the line source is a rotatable air-copper-lead cylinder that is used to provide varying degrees of TCT beam attenuation. During the emission scan, the cylinder can be dialed to the lead sector to effectively "turn off" the TCT beam and thus eliminate contamination of the emission data. A stacked lead

foil ("multislat") collimator is positioned adjacent to the cylinder and provides collimation of the TCT beam in the axial direction for the reduction of detected scatter events (Fig. 2 in [5]). This system design has been issued a U.S. Patent (Number 52890080).

The TCT data were acquired of plastic rod and anthropomorphic thorax phantoms to investigate the capability of the line source and rotatable air-copper-lead attenuators to determine attenuation maps. The phantoms were also scanned using a curved transmission slab source mounted to a parallel-hole collimator. The fan-beam TCT images demonstrated improved resolution and noise characteristics compared with the parallel-beam TCT images (Figs. 4 and 5 in [5]).

Two patient scans also were performed to evaluate the clinical usefulness of the fan-beam TCT system. Both patients were female, one weighing 140 pounds, the other, 114 pounds. The resulting TCT images from both patients demonstrated high resolution, low noise characteristics and allowed visualization of ribs, spinal column, and vertebra (Figs. 8 and 9 in [5]). For one of the patients the TCT image was truncated due to the limited field-of-view. An evaluation of the resulting nonuniform attenuation compensated SPECT images showed an improvement relative to SPECT images with uniform or no attenuation compensation (Fig. 10 in [5]).

In an effort to find a radionuclide with improved characteristics for a gamma TCT source, we investigated the use of a tellurium-123m line source to determine attenuation maps for SPECT reconstruction [15]. Tellurium-123m has a primary photon energy of 159 keV which is ideal for detection by conventional gamma cameras. The half life of Te-123m is 119.7 days which gives it an important advantage over Tc-99m in terms of the frequency with which the source must be replenished. For the prototype line source, the Te-123m was produced at the High Flux Isotope Reactor and fabricated into a line source at the Radiochemical Engineering Development Center at the Department of Energy's Oak Ridge National Laboratory (ORNL). The line source is housed in a double-wall, welded stainless steel tube for radiation safety and is composed of a compact stack of 41 aluminum-tellurium pellets, each with a diameter of 2 mm and a length of 2 mm.

The experimental evaluation of the Te-123m TCT line source was performed with both anthropomorphic phantom and patient data using the acquisition system described above. For both phantom and patients studies, a 20 minute long scan and a 2 minute short scan were acquired with an energy window centered at 159 keV and 15% width. At the time of the study the activity of the line source was estimated to be 1,443 MBq (39 mCi). In the reconstructed phantom TCT images (Fig. 2 in [15]), the attenuation coefficients were found to be within 5% of the narrow beam values in the soft tissue, lung, and bone regions (Table II in [15]). The reconstructed patient TCT images (Fig. 3 in [15]) showed high resolution, low noise quality and the sternum, spine and ribs were clearly visible. The average attenuation coefficient in the heart region was found to be 0.146 cm^{-1} which is close to the narrow beam value for soft tissue at 159 keV.

This first prototype Te-123m source was relatively expensive ($15,700) because of the cost of the enriched Te-122 used as the target material, the sophisticated wet radiochemistry had to be performed in special hot chemistry hoods, and because of the extra care that was used in making the Te pellets. We are collaborating with Oak Ridge personnel (C. Alexander) to investigate innovative approaches to reduce to manufacturing costs. Since only a very small fraction (<0.02%) of the Te-122 is converted to Te-123m during neutron activation, the source may be reprocessed, at a modest additional cost (perhaps less than four or five thousand dollars), after initial decay of the Te-123m. Therefore, the pro-rated cost of the Te-123m source over several years, may be clinically acceptable. We are comparing the Te-123m source with a Gd-153 source which emits 100 keV photons. Although the Gd-153 source is less expensive, there will be more contamination from Tc-99m photons that have downscattered into the Gd-153 photopeak. A correction for these contaminating photons must be performed.

The transmission computed tomography project was supported approximately equally by this DOE grant (DE-FG05-89ER60894) and by a grant from the NIH (CA33541). The Te-123m line source ($15,700), rotatable holder ($5,000), and the long focal length fan beam collimator ($7,000) were developed and built with funds provided by the DOE grant, while most of the TCT software (including clinical applications such as myocardial imaging, etc.) were supported by the NIH grant.

1.2.3. Determining the accuracy of SPECT to quantify I-123 and At-211

Substantial progress has been made in this area during the last project period and is summarized in the first section below. While our initial aim was to compare SPECT quantification of I-123 with PET quantification of I-124, due to the funding cut-back, this goal could not be achieved. However, we were able to develop important image registration tools that will facilitate attaining this goal in the future. A summary of our development and evaluation of image registration techniques is included the second section.

SPECT quantification of I-123 distribution. Considerable progress has been made during the previous project period on developing and evaluating SPECT methods for the quantification of I-123 distribution. Three studies in this area are described here.

The goals of the initial study [9] were to investigate the effect of septal penetration on I-123 SPECT activity quantification using low energy, high resolution collimators, and to evaluate a semi-automatic method for measuring volume and activity of I-123 distribution with SPECT. The results have implications for radiolabeled monoclonal antibody imaging and in dosimetry determination for cancer treatment. Data were acquired of experimental phantoms containing spheres filled with high purity I-123 solution. The penetration study compared the reconstructed activity of a 3.4 cm diameter sphere with and without the presence of surrounding activity (Fig. 2 in [9]). In the study of volume and activity quantification, three different size spheres (diameters of 1.8 cm, 2.8 cm, and 3.4 cm) were imaged in three different sphere:background (S:B) I-123 concentration ratios (2.5, 5, and 10) with low energy collimators. The filtered backprojection reconstruction method was used with compensation for scatter, attenuation, and detector response. Volume and activity measurements were obtained from the SPECT image using a semi-automatic gradient technique which estimates the location of the sphere/background boundary in three dimensions.

With the low energy collimator, there was only a small (less than 2%) increase in the measured activity of the sphere when surrounding activity was present. The measured volume for the two largest spheres was within 5% of the true volume for all S:B ratios (Table 1 in [9]). The activity measurement of these spheres was consistently underestimated by 20-25% but suggested that the accuracy could be improved with calibration. For the smallest sphere, the volume was grossly overestimated and only at the 10:1 (S:B) ratio was the activity measured reasonably accurately (<20%). We concluded from this study that these low energy collimators are suitable for quantitative I-123 SPECT. Also, accurate SPECT volume and activity quantification of I-123 distribution can be achieved by semi-automatic means at clinical count densities for objects as small as 2.8 cm in diameter and reasonable activity quantification is possible for smaller objects with an S:B ratio of at least 10.

The second Sand biological half-life of theion of I-123 distribution [12] employed a model-based approach to estimate intratumor activity from quantitative filtered backprojection SPECT reconstructions. Tumor activity in a SPECT image is modeled as a blurred version of uniform activity in concentric spherical shells. The shell activities are estimated by a least squares procedure using an estimate of the blurring function. This method was evaluated using Monte Carlo simulated data of 1.25 and 2.0 cm radius tumors which were uniform or consisted of a lower activity core and a higher activity shell. The tumors were located in a water-filled cylinder with shell:background and shell:core activity ratios of 4:1. Projection data at clinical count levels were simulated and images were reconstructed by filtered backprojection with compensation for attenuation, scatter and detector response.

For the 2.0 cm radius tumors, shell activity was recovered to within about 25% and core activity to within about 50% (Tables 2-6 in [12]). For the 1.25 cm radius tumors, shell activity was estimated to within about 50% but core activity estimates were unreliable. Factors contributing to errors in intratumor activity estimates were limited SPECT spatial resolution compared with the small tumor sizes, image noise due to limited projection counts, and the anisotropic and spatially-varying character of the SPECT point source response function. We have concluded that a model-based approach is superior to not using a model-based approach. We intend to investigate these approaches and compare them with formal Bayesian methods during the next project period.

The final study in this area evaluated I-123 SPECT volume and activity quantification in terms of accuracy and precision using an ensemble of experimental phantom data [13]. Two reconstruction methods were considered: the filtered backprojection (FBP) method with 2D Metz pre-filtering and single iteration Chang attenuation compensation, and an iterative ML-EM method that used Gaussian post-filtering and incorporated the 3D divergent detector response and attenuation in the detection kernel. Both methods were examined over a range of resolution and noise characteristics. An ensemble of 21 SPECT data sets were acquired of a cylindrical phantom that contained spheres of size 21.4, 12.0, and 5.7 ml, filled with high purity I-123 in a uniform background (5:1 uptake ratio). Each data set was reconstructed by both methods, and sphere volume and activity measurements were obtained from reconstructions using a semi-automatic method that defines the region-of-interest based on the intensity gradient in the area of increased I-123 concentration. The mean and standard deviation of the 21 measurements provided accuracy and precision indices, respectively.

For the 21.4 ml sphere, the measured volume with either reconstruction method was accurate to within 5% of the true volume with a standard deviation of approximately 8% of the true volume. For the 12.0 ml sphere the measured volume with the iterative method exhibited substantially smaller standard deviation for

equal accuracy compared with the FBP method. Sphere activity was underestimated with both methods due to spatial resolution effects. The 5.7 ml sphere was generally below the size limit for volume and activity quantification by these methods.

SPECT quantification of At-211 distribution. Our initial efforts directed toward the ultimate goal of using pinhole collimation to image brain tumors with radiolabeled therapeutic MAbs focused on SPECT quantification with At-211 using medium energy parallel hole collimators. These studies are described in the next section below. The initial use of the parallel hole collimators provided a reference upon which future results with pinhole collimators could be evaluated. The objective of this first study using At-211 [3] was to investigate the capability of standard SPECT techniques to quantitatively and qualitatively image this radionuclide. The At-211 was produced on the Duke University Medical Center CS-30 cyclotron using the Bi-209(α,2n)At-211 reaction by bombarding a natural bismuth metal target with 28 MeV α particles. Four small glass vials were filled with increasing volumetrically measured activities in the ratio 1:2:3:4. Vial activities were measured in a dose calibrator then allowed to decay to reach levels of 0.126, 0.270, 0.396, and 0.522 MBq (3.4, 7.3, 10.7, 14.1 μCi). These vials were placed in a cylindrical Lucite phantom, and the phantom was scanned both empty (vials only) and water-filled. An additional cold rod SPECT phantom was scanned for qualitative evaluation. The SPECT data were reconstructed by FBP using Chang multiplication attenuation compensation (water-filled phantom only) with a measured linear attenuation coefficient and dual window scatter subtraction using a scatter energy window 35% in width located below the photopeak energy window.

The results from the quantitative study showed that the ratio of the measured vial activity from the SPECT image agreed closely with the dose calibrator (Table 2 in [3]). In addition, the attenuation and scatter corrections put the in-water measurements in very close agreement with the in-air measurements. With the cold rod phantom, the largest rods (12.7 mm separation) were visible.

The objective of the second study [11] of At-211 SPECT quantification was to evaluate SPECT and two planar imaging methods, geometric mean (GM) and buildup factor (BF), for their potential to quantify *in vivo* At-211 distributions in rat spinal subarachnoid spaces using phantom studies. A potential application is the intrathecal administration of At-211-labeled radiopharmaceuticals for the treatment of neoplastic meningitis, a particularly devastating malignancy spread along the surface of the spinal cord. A rat spinal canal phantom (Fig. 1 in [11]) consisted of a 5 cm o.d. (3 mm wall) x 15 cm long acrylic cylinder "body" with a "spinal canal" insert made from a 9 cm length of 1 ml polystyrene pipette having a 3 mm i.d. Activity quantification of structures this small poses significant difficulties. The canal:background activity ratios that were considered included 1:0, 15:1, 20:1, 50:1, and 100:1. The absolute activity used in the canals ranged from 0.56-1.11 MBq (15 to 30 μCi). Medium energy collimators were used along with standard acquisition parameters. Because of the effects of spatial resolution and small canal size, accurate quantification of intracanal activity requires a region of interest much larger than the canal diameter. A detailed description of the region of interest methods can be found in [11].

The results of the activity quantification for canal:background ratios of 50:1 and 100:1 showed systematic errors within 10% for SPECT and BF but were as large as 31% for GM (Table 1 in [11]). Errors increased to 23, 25 and 45% for SPECT, BF, and GM, respectively, for the 15:1 configuration. All methods were within 10% for the no background case. Corrected SPECT activities based on the known canal size (3 mm diameter) and estimated background level showed that the systematic errors were reduced to less than 10% in all cases (Table 2 in [11]). We conclude that reasonable quantification accuracy of intracanal At-211 distributions is possible using standard gamma camera planar or SPECT imaging methods along with the region of interest approach presented here.

1.2.4. Development of image registration methods

Two studies were performed in the area of image registration. The objective of the first study [4] was to measure the accuracy of a surface-fitting algorithm for three-dimensional image registration of SPECT, PET, and MR images. In order to provide an ideal case in which underlying surface structures matched identically, a three-dimensional brain phantom was scanned using the three modalities, and the surface-fitting technique was applied. Fiducial markers attached to the outside of the phantom were used to measure error in the registration. Since registration quality depends on surface definition, an edge determination method was used which leads to improved surface matching and requires little operator interaction.

The phantom was filled with agents appropriate for each study. For MRI, the phantom and markers were filled with 0.16 M $CuSO_4$ solution. For SPECT, the phantom contained 1100 MBq (30 mCi) Tc-99m solution and the markers each contained 0.7 MBq (19 μCi). For PET, the phantom was filled with 220 MBq (6 mCi) F-18-2-fluoro-2 deoxyglucose (FDG) solution and the fiducial markers contained 0.11 MBq (3 μCi) FDG. For each modality the phantom was scanned using standard acquisition parameters. The method of

edge determination for each data set is described in detail in [4]. The surface fit technique developed by Pelizzari et al. (Pelizzari et al. 1989) was used to match each PET and SPECT surface to the MR surface.

The results indicated that overall translational errors were less than 2 mm for most regions and rotational errors less than 2 degrees in all cases (Table 4 in [4]). Errors for specific internal regions were also determined to be less than 2 mm for most regions, with only a few fits resulting in errors greater than 3 mm for some cortical regions. We conclude that surface fitting is sufficiently accurate for visual comparison of registered images and for enhanced SPECT and PET region of interest determination and image reconstruction.

In the second image registration study [10], the accuracy of the surface-fitting image registration technique described above was investigated for matching F-18-FDG and O-15-H_2O PET brain images with MR images in patients. The use of partial brain surfaces (a single hemisphere or a limited number of slices) was investigated to simulate cases in which severe brain defects or limited axial field of view would preclude using the entire brain surface. Three F-18-FDG and three O-15-H_2O scans were performed on five volunteers, in addition to volume MR studies. Standard PET acquisition parameters were used, and the FDG dose was 366 MBq (10 mCi). Both T1 and T2 weighted volume protocol acquisitions were used for MR. Simple thresholding was used to determine edges for the MR data, and a first derivative maximum criterion described in detail in [10] was used for the PET data. Fiducial markers were placed on the subjects' scalps to provide references for registration accuracy.

The surface-fitting technique worked well in all cases, with only 1% scaling necessary for the best fit. Errors in fiducial marker positions between MR and transformed PET were less than 2 mm in the transverse directions and less than 4.5 mm in the axial direction (Table 4 in [10]). Also, fits based on the partial surfaces worked well and gave results very similar to the full brain fits (Table 5 in [10]). We conclude that the surface-fitting technique is accurate for FDG and H_2O PET studies, even when part of the brain surface cannot be used.

1.2.5. Investigating SPECT imaging of radiolabeled MAbs using pinhole collimation

SPECT quantification using pinhole collimation. The objective of this initial investigation using pinhole SPECT [7] was to evaluate small field-of-view, ultra-high resolution pinhole collimation for a rotating camera SPECT system that could be used to image small laboratory animals. Since geometric efficiency increases markedly for points close to the pinhole, small-diameter and high magnification pinhole geometries may be useful for selected imaging tasks when used with large field-of-view scintillation cameras. The use of large magnifications can minimize the loss of system resolution caused by the intrinsic resolution of the scintillation camera. A pinhole collimator was designed and built that can be mounted on one of the scintillation cameras of a triple-head SPECT system. Three pinhole inserts with approximate aperture diameters of 0.6, 1.2, and 2.0 mm were built and can be mounted individually on the collimator housing (Figs. 1 and 2 in [7]).

Planar system efficiency and spatial resolution were measured using small point and line sources, respectively. The results with the pinhole collimators were compared to high energy, parallel hole collimators. In order to evaluate SPECT image quality with the pinhole collimators, a "micro-cold rod" phantom was used which contained six sets of solid plastic rods having diameters of 1.2, 1.6, 2.4, 3.2, 4.0 and 4.8 mm. The center-to-center spacing between the adjacent rods is twice the rod diameter. The Tc-99m radionuclide was used for all phantom studies. Two female rats were also imaged with the pinhole collimator. One rat (325 g) was used to acquire a bone scan using Tc-99m-labeled MDP, the other rat (315 g) was used to acquire a liver scan using Tc-99m-labeled sulfur colloid. SPECT data were reconstructed using both a 3D FBP algorithm and an iterative ML-EM algorithm.

The results of the measured planar resolution (Fig. 5 in [7]) showed better resolution for all three pinhole collimators compared with the parallel hole collimator. The efficiency (Fig. 6 in [7]) for the pinhole collimators decreased with distance from the camera. Reconstructed SPECT resolutions (near the AOR) for the 0.6, 1.2, and 2.0 mm pinhole apertures were equal to 1.5, 1.9, and 2.8 mm, respectively, at an ROR of 4 cm. In the SPECT reconstructions of the pinhole data, the FBP and ML-EM algorithms both clearly visualized the 1.6 mm diameter rods of the micro-cold-rod phantom (Fig. 7 in [7]). In the pinhole SPECT bone scans of the first rat (Fig. 9 in [7]), the bones in the skull and mandible were visualized. In the liver scan of the second rat (Fig. 10 in [7]), the hepatic anatomy was well visualized with areas of absent activity secondary to vascular structures. We conclude that ultra-high resolution pinhole SPECT is an effective and practical method for imaging small animals and can be readily used with existing rotating camera SPECT systems.

The objective of the second set of experiments was to experimentally investigate the potential capability of ultra-high pinhole (1 mm dia. aperture) SPECT to quantify compartmentally administered brain tumor activities. In this initial study Tc-99m was used to obtain baseline data which has not been affected by high

energy photon penetration through the aperture edges. These data would be useful for evaluating the effectiveness of the proposed approaches that will be implemented to reduce the effect of penetration.

Two experiments were performed. The first study was a high count density scan of a micro-cold rod phantom (rod dia.: 1.2, 1.6, 2.4, 3.2, 4.0, and 4.8 mm) placed at 11 cm from the pinhole aperture. SPECT data were acquired using linear and angular sampling intervals of 1.0 mm (at the AOR) and 2 deg., respectively. A ramp filter was used to reconstruct the SPECT image, and a first order Chang attenuation compensation was performed (Fig. 3). Four sectors are visualized in the image. We believe that the increased count density observed in the center of the image results from absorption of Tc-99m pertechnetate onto the surface of the single 6.4 mm nylon bolt that was used to secure the rod insert to the cylinder.

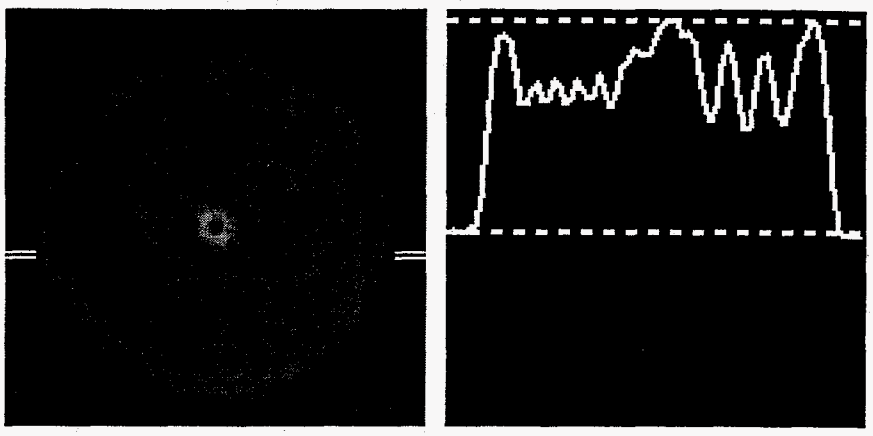

Figure 3. Pinhole SPECT image of micro cold rod phantom (ROR = 11 cm).

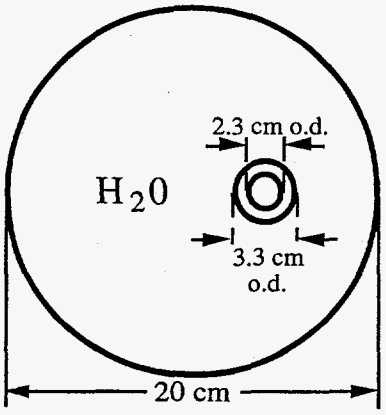

Figure 4. Magnified SPECT transaxial images of shell/core insert. [(left) 5:1 image, (middle) 3:1 image, (right) 1.5:1 image] A diagram of the complete phantom is shown on the right. The lines in the images indicate the locations of the horizontal (middle row) and vertical (bottom row) profiles.

The next experiment consisted of SPECT pinhole scans of a small spherical shell/core phantom (Fig. 4) placed in a water-filled, brain-sized cylinder. This phantom was used to simulate the activity distribution of an intratumorally administered agent. The phantom is made of 2.3 cm o.d. hollow polycarbonate sphere positioned within a 3.3 cm o.d. polycarbonate hollow sphere. The wall thickness of the plastic spheres is about 1 mm, the core diameter is 2.1 cm, and the shell thickness is 4 mm. Three different shell:core activity ratios (5:1, 3:1, 1.5:1) were used. The core/shell phantom was filled with thirty to 45 mCi of Tc-99m, which is similar to the amount of I-131 that might be used for radioimmunotherapy. The phantom was scanned for 15 minutes using the 1 mm pinhole mounted on a single head of a triple camera SPECT system. A ramp filter was used to reconstruct the SPECT images, and a first order Chang attenuation compensation was performed. Scatter compensation was performed using a dual window scatter subtraction method (Jaszczak et al. 1984) . The scatter data was reconstructed using a Hann filter (cutoff = Nyquist freq.), and a value of

k = 0.45 (determined by scanning a point source in air and in water) was used for the scatter subtraction constant. Centrally located transaxial images and profiles are shown in Fig. 4. The 1 mm thick plastic wall of the inner sphere is visualized in the image and profiles of the 1.5:1 ratio scan.

Region of interest (ROI) analysis was used to quantitatively determine absolute activities and concentrations (Tables 4-6). A point source containing a known amount of activity was imaged in air at the AOR to calibrate system sensitivity. The measured activities within the shell/core phantom and the measured concentrations within the core are within 3% of the true activities. The measured concentrations within the shell are about 17% less than the true concentrations because of the effect of finite spatial resolution and object size. These results demonstrate the potential effectiveness of pinhole SPECT to determine quantitative biodistribution data of intratumorally administered radiolabeled agents. An objective of this proposal is to demonstrate this capability using the clinically appropriate radionuclide I-131.

TABLE 4. Total Activity Measurements.

Activity Ratio (Shell : Sphere)	Total Activity (mCi)	Measured (mCi)	Relative Error (%)*
5.0 : 1	44.6	43.7	-2
3.0 : 1	29.5	30.0	+2
1.5 : 1	36.7	37.7	+3

TABLE 5. Concentration Measurements (Spherical core).

Activity Ratio (Shell : Sphere)	True Concentration (mCi/cm^3)	Measured Concentration† (mCi/cm^3)	Relative Error (%)*
5.0 : 1	0.71	0.69	-3
3.0 : 1	0.74	0.73	-1
1.5 : 1	1.64	1.64	0

TABLE 6. Concentration Measurements (Shell).

Activity Ratio (Shell : Sphere)	True Concentration (mCi/cm^3)	Measured Concentration‡ (mCi/cm^3)	Relative Error (%)*
5.0 : 1	3.45	2.79±0.06	-19
3.0 : 1	2.20	1.75±0.11	-20
1.5 : 1	2.47	2.08±0.05	-16

*Relative Error = (measured - true) / true *100%
†Circular Region-of-interest = 1.87 cm diameter.
‡Averaged over six small square region-of-interest. (ROI = 0.25 cm x 0.25 cm).
The standard deviations are also given.

The objective of the third investigation using pinhole SPECT [14] was to compare the use of pinhole collimation relative to medium energy, parallel hole collimation for SPECT imaging of the head with In-111. Two pinhole inserts adaptable to the collimator housing were designed and built with aperture diameters of 4.5 and 6.0 mm. The collimator focal length was 15.0 cm and the acceptance angle was 114 degrees. Planar and SPECT sensitivity and resolution measurements were performed using point and line sources filled with aqueous In-111 solution. Measurements were made with both pinhole inserts as well as the medium energy collimator. A cold rod SPECT phantom was used for a qualitative comparison between pinhole SPECT images and those obtained with medium energy collimation. A hot sphere phantom was used to evaluate the quantitative capabilities of pinhole SPECT using Chang attenuation correction and scatter subtraction compensation. This phantom consisted of 4 hot spheres of various sizes contained in a 20 cm diameter cylinder with a uniform background activity and a 2.2:1 sphere:background uptake ratio. All SPECT images were reconstructed using a 3D pinhole FBP method.

The results of the measured planar spatial resolution and sensitivity (Figs. 8 and 9 in [14]) and SPECT resolution and sensitivity (Figs. 10 and 12 in [14]) for the pinhole and medium energy collimators showed that for scans of In-111 in the head, pinhole collimation can offer advantages in spatial resolution and/or sensitivity compared with medium energy collimation. Transaxial slices (1.1 cm thickness) of the cold rod phantom reconstructed from 4.5 mm pinhole data and medium energy collimator data (Fig. 12 in [14]) show clearly improved quality with pinhole collimation. More and smaller rods can be visualized and rod to background contrast is higher in the pinhole images. The results with the hot sphere phantom data likewise demonstrate superior quality with pinhole collimation (Fig. 13 in [14]). The quantitative results of sphere activity (Table 1 in [14]) indicated an accuracy within 15% was possible for measurement of total activity for all spheres. Activity concentration was significantly underestimated in these spheres due to spatial resolution effects. We conclude from this study that pinhole SPECT can be a useful approach for imaging medium-energy radionuclides in the head.

SPECT imaging of iodine-131 distribution in the head. In the treatment of gliomas and other types of intracranial tumors, recent studies have demonstrated the potential of radioimmunotherapy (RIT) using compartmentally-administered I-131 as an alternative to surgery, chemotherapy, or external beam radiation (Lee et al. 1988; Zalutsky et al. 1989). Dose determination with RIT requires accurate estimation of the *in vivo* spatial and temporal distribution of the I-131-labeled radiotherapeutic agent. Quantification of the I-

131 distribution with SPECT is challenging due to the 364 keV primary photon emission (82% abundance) and the accompanying high energy gamma rays at 637 keV (6.5%) and 723 keV (1.7%). This study investigated the use of pinhole collimation for I-131 SPECT and compared the results with medium and high energy parallel hole collimation in terms of SPECT image quality and quantitative accuracy with experimental phantom data.

A prototype pinhole collimator was constructed of lead with a 3.0 mm hole diameter, a 16 cm focal length (aperture to crystal distance), and 100 degree acceptance angle. The medium energy, parallel hole collimator (MEPAR) had 3.25 mm hole diameter, 59.0 mm hole length, and 1.17 mm septal thickness. The respective parameters for the high energy, parallel hole collimator (HEPAR) were 3.8 mm, 78 mm, 1.8 mm. Point and line I-131 sources were used to measure sensitivity and resolution, respectively, and a simple head phantom was used to evaluate reconstructed image quality and quantitative accuracy. The head phantom consisted of 5 cylindrical glass vials of varying size and I-131 concentration (Fig. 5, Table 7). The vials were placed inside a 20.2 cm diameter water-filled cylinder. The pinhole and MEPAR data were each acquired on a single head of a triple-camera SPECT system, and the HEPAR data were acquired on one head of a dual-camera SPECT system (Trionix Research Laboratories Inc.). The primary energy window was 364 keV ± 9%, and for the head phantom a secondary energy window (282 keV ± 18%) was acquired for scatter compensation. The scan time for the head phantom acquisition with each collimator was one hour.

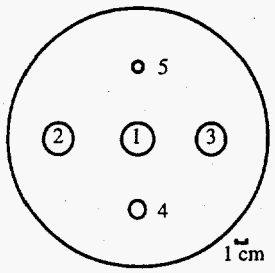

Figure 5. Head phantom

TABLE 7. Head phantom description

vial	i.d. (mm)	total μCi	μCi/ml
1	25	1236	49.4
2	25	619	24.7
3	25	309	12.3
4	13	454	94.5
5	9	155	73.8

The measured point source sensitivity (cnts·sec^{-1}·μCi^{-1}) at 13.5 cm distance was 0.705 for MEPAR, 0.442 for HEPAR, and 0.850 for pinhole. The planar resolution (FWHM) at this distance was 12.5 mm for MEPAR, 12.5 mm for HEPAR, and 12.0 mm for pinhole. The on-axis SPECT resolution (13.5 cm radius of rotation) was 14.3 mm for MEPAR, 13.1 mm for HEPAR, and 13.1 mm for pinhole. The 8 cm off-axis SPECT resolution in a radial profile was 14.3 mm for MEPAR, 13.4 mm for HEPAR, and 6.7 mm for pinhole. The same in a tangential profile was 11.7 mm for MEPAR, 10.1 mm for HEPAR, and 11.8 mm for pinhole.

All reconstructions used the filtered backprojection method (FBP) using a ramp filter with cutoff at the Nyquist frequency. For the pinhole data, a 3D FBP algorithm based on the method of Feldkamp (Feldkamp et al. 1984) was used. The head phantom data were smoothed prior to reconstruction using a 2D Hann window with cutoff at the Nyquist. Multiplicative Chang attenuation compensation (Chang 1978) was used with this data, assuming a linear attenuation coefficient (for 364 keV photons) of 0.11/cm, and Jaszczak scatter compensation (Jaszczak et al. 1984) was performed with the k factor equal to 0.5. The k factor was obtained from evaluation of point source images in air and in water. Total activity was measured for each vial in the SPECT images using a threshold of 10% of the peak counts within an ROI. A point source calibration factor (cnts·sec^{-1}·μCi^{-1}) was determined for each collimator. The SPECT-measured activities were compared to well-counter results of solution samples.

The reconstructed images from the three collimators are shown in Fig. 6. Figure 7 shows the horizontal and vertical profiles through the reconstructed vial activity in these images. The profiles show the effects of septal penetration in the MEPAR image as an elevated activity level between the vials and a reduced contrast. The vertical profiles reveal that relative to the parallel hole images the pinhole image gives a more accurate activity concentration in the two smaller, off-axis vials. However, in the pinhole image the activity concentration of the larger, on-axis vial is slightly below the true concentration (see Table 7). The quantitative analysis is illustrated in Table 8. All three collimators provided reasonable quantitative accuracy (less than 12% error). For the smallest vial, the pinhole collimator had slightly improved accuracy relative to the parallel hole collimators.

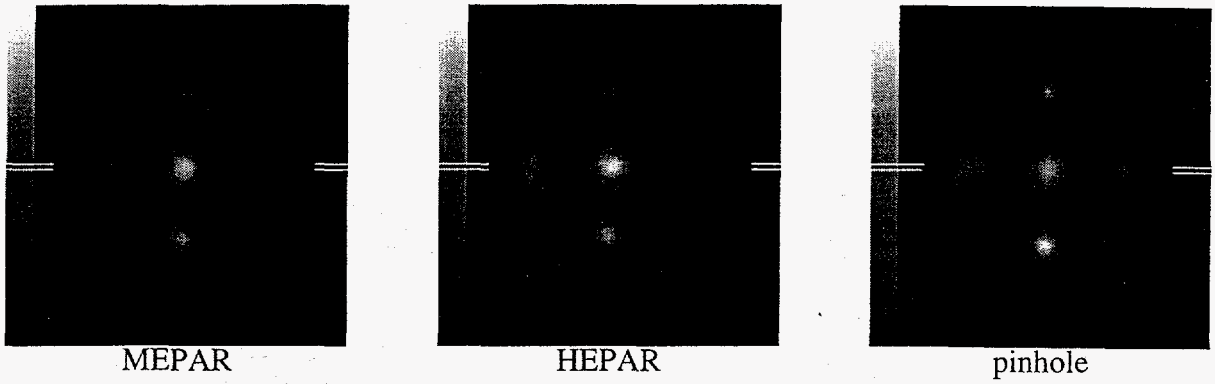

Figure 6. Reconstructed images with the three collimators.

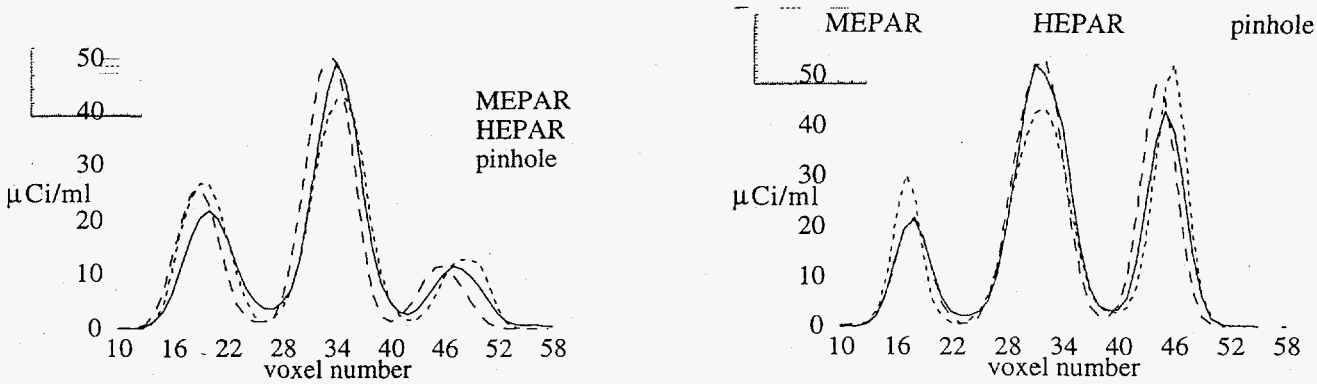

Figure 7. Horizontal (left) and vertical (right) profiles. Vertical profile begins at top of image.

Table 8. SPECT-measured total vial μCi (% error)

collimator	vial 1	vial 2	vial 3	vial 4	vial 5
Actual	1236	619	309	454	155
MEPAR	1237 (0.8)	648 (5.4)	333 (8.5)	427 (-5.3)	136 (-12.)
HEPAR	1261 (2.7)	643 (4.4)	285 (-7.2)	456 (1.1)	139 (-9.7)
pinhole	1251 (1.9)	689 (12.)	320 (4.2)	455 (0.8)	146 (-5.2)

The summary and conclusions from this study are the following:

1. The pinhole collimator demonstrated superior resolution/sensitivity trade-off relative to the medium and high energy parallel hole collimators over source-to-collimator distances relevant in head imaging.
2. The medium energy collimator exhibited substantial septal penetration effects that reduced the contrast of the reconstructed vial activity although it did not greatly affect the SPECT-measured vial activity.
3. The SPECT-measured total activity was comparable for all collimators. Profiles showed the reconstructed activity with the pinhole collimator was more accurate for the smaller, off-axis vials and less accurate for the larger, on-axis vial.

Monte Carlo modeling of penetration effects for iodine-131 pinhole imaging. The objective of this study was to account for penetration of high energy photons near the edges of a pinhole aperture. At 364 keV, the effective hole size is no longer accurate for determining the performance of a pinhole collimator including resolution and efficiency in collimator design. The inaccuracy is due to marked penetration at the knife edge of the pinhole. We have modified our existing Monte Carlo program (Wang et al. 1993) to model the penetration effect. Forced detection is employed for sampling of the emission direction of a primary photon to increase simulation efficiency (Fig. 8). An experiment using a lead pinhole was performed to validate the Monte Carlo modeling (Fig. 9). The pinhole had a physical hole size of 1.5 mm, and a span (cone) angle of

the knife edge of 100 degrees. A point source was located at 3 and 18 cm on the principal ray from the pinhole aperture for data acquisition. The comparison between simulated and experimentally acquired data demonstrates the accuracy of our Monte Carlo modeling (Fig. 10). We propose to use this Monte Carlo model to design and evaluate new geometries for pinhole collimation. In addition, the model will be useful for the development and evaluation of algorithms to compensate for photon penetration in reconstructed SPECT images.

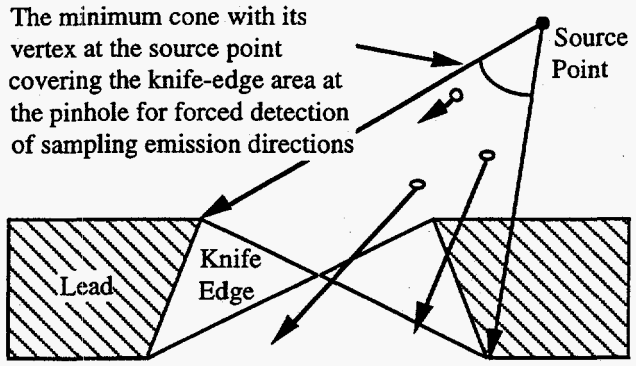

Figure 8. Cone angle used for forced detection.

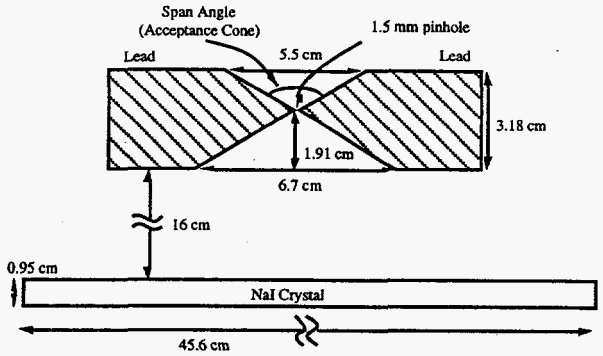

Figure 9. Pinhole aperture specifications.

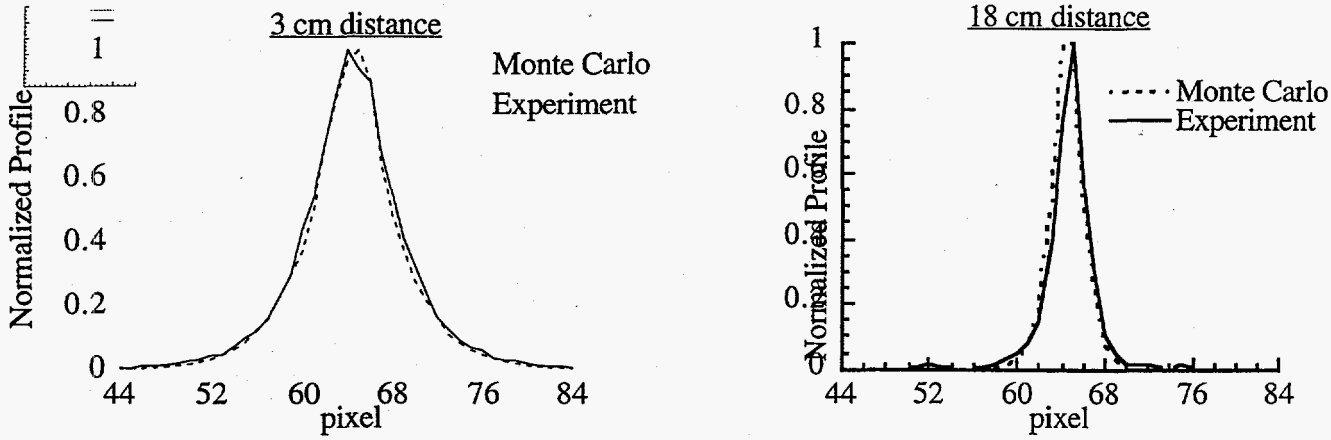

Figure 10. Normalized profiles through point source images.

1.3. PUBLICATIONS

1.3.1. Peer-reviewed Journal Articles Supported Fully or Mainly by this Grant Since The Application Was Last Submitted for Competitive Renewal (3/92 - 5/95)

1. Turkington TG, Jaszczak RJ, Greer KL, Coleman RE: Correlation of SPECT images of a three-dimensional brain phantom using a surface fitting technique. *IEEE Trans Nucl Sci* 39(5):1460-1463, 1992.
2. Gilland DR, Jaszczak RJ, Bowsher JE, Turkington TG, Liang Z, Greer KL, Coleman RE: Quantitative SPECT brain imaging: Effects of attenuation and detector response. *IEEE Trans Nucl Sci* 40(3):295-299, 1993.
3. Turkington TG, Zalutsky MR, Jaszczak RJ, Garg PK, Vaidyanathan G, Coleman RE: Measuring astatine-211 distributions with SPECT. *Phys Med Biol* 38:1121-1130, 1993.
4. Turkington TG, Jaszczak RJ, Pelizzari CA, Harris CC, MacFall JR, Hoffman JM, Coleman RE: Accuracy of registration of PET, SPECT, and MR images of a brain phantom. *J Nucl Med* 34:1587-1594, 1993.
5. Jaszczak RJ, Gilland DR, Hanson MW, Jang S, Greer KL, Coleman RE: Fast transmission CT for determining attenuation maps using a collimated line source, rotatable air-copper-lead attenuators, and fan beam collimation. *J Nucl Med* 34:1577-1586, 1993.
6. Turkington TG, Gilland DR, Jaszczak RJ, Greer KL, Coleman RE, Smith MF: A direct measurement of skull attenuation for quantitative SPECT. *IEEE Trans Nucl Sci* 40(4):1158-1161, 1993.
7. Jaszczak RJ, Li J, Wang H, Zalutsky MR, Coleman RE : Pinhole collimation for ultra-high resolution, small-field-of-view SPECT. *Phys Med Biol* 39:425-437, 1994.
8. Gilland DR, Jaszczak RJ, Wang H, Turkington TG, Greer KL, Coleman RE: A 3D model of non-uniform attenuation and detector response for efficient iterative reconstruction in SPECT. *Phys Med Biol* 39:547-561, 1994.
9. Gilland DR, Jaszczak RJ, Turkington TG, Greer KL, Coleman RE: Volume and activity quantitation with Iodine-123 SPECT. *J Nucl Med*, 35:1707-1713, 1994.
10. Turkington TG, Hoffman JM, Jaszczak RJ, MacFall JR, Harris CC, Kilts CD, Pelizzari CA, Coleman RE: Accuracy of surface fit registration for PET and MR brain images using full and incomplete brain surfaces. *J Comp Assist Tomogr*, 19(1):117-124, 1995.
11. Johnson EL, Turkington TG, Jaszczak RJ, Gilland DR, Vaidyanathan G, Greer KL, Coleman RE, Zalutsky MR: Quantitation of ^{211}At in small volumes for evaluation of targeted radiotherapy in animal models. *Nucl Med and Biol* 22(1):45-54, 1995.
12. Smith MF, Gilland DR, Jaszczak RJ, Coleman RE: Estimation of tumor activities from simulated I-123 SPECT studies. *IEEE Trans Nucl Sci,* in press, 1995.
13. Gilland DR, Jaszczak RJ, Greer KL, Coleman RE: Measured accuracy and precision in quantitative SPECT imaging with Iodine-123. *IEEE Trans Nucl Sci,* in press, 1995.
14. Johnson EL, Jaszczak RJ, Wang H, Li J, Coleman RE: Pinhole SPECT for imaging In-111 in the head. *IEEE Trans Nucl Sci,* in press, 1995.
15. Wang H, Jaszczak RJ, McCormick JW, Greer KL, Coleman RE: Experimental evaluation of a Tellurium-123m transmission source to determine attenuation maps for SPECT. *IEEE Trans Nucl Sci,* in press, 1995
16. Johnson EL, Wang H, McCormick JW, Greer KL, Coleman RE, Jaszczak RJ: Pixel driven implementation of filtered backprojection for reconstruction of fan beam SPECT data using a position dependent effective projection bin length. *Phys Med Biol*, submitted, 1995.
17. McCormick JW, Gilland DR, Jaszczak RJ, Greer KL, Coleman RE: The effect of registration errors between transmission and emission scans on a SPECT system designed for fast sequential scanning. *Phys Med Biol.* submitted, 1995.

1.3.2. United States Patents supported fully or mainly by this grant since the application was last submitted for competitive renewal (2/92-5/95)

18. Jaszczak RJ, Gilland DR: Method and apparatus for enhanced single photon tomography. United States Patent Number 5289008, 1994.

1.3.3. Directly Related Peer-Reviewed Publications Supported in Part by this Grant Since the application was last submitted for competitive Renewal (3/92 - 5/95)

19. Jaszczak RJ, Li J, Wang H, Greer KL, Coleman RE: Three dimensional reconstruction of combined cone beam and parallel beam data. *Phys Med Biol* 37:535-548, 1992.

20. Liang Z, Turkington TG, Gilland DR, Jaszczak RJ, Coleman RE: Simultaneous compensation for attenuation, scatter, and detector response of SPECT reconstruction in three dimensions. *Phys Med Biol* 37:587-603, 1992.
21. Smith MF, Floyd CE, Jaszczak RJ, Coleman RE: Three dimensional photon detection kernels and their application to SPECT reconstruction. *Phys Med Biol* 37:605-622, 1992.
22. Smith MF, Floyd CE, Jaszczak RJ, Coleman RE: Reconstruction of SPECT images using generalized matrix inverses. *IEEE Trans Med Imaging* 11:165-175, 1992.
23. Smith MF, Floyd CE, Jaszczak RJ, Coleman RE: Evaluation of projection pixel-dependent and pixel-independent scatter correction in SPECT. *IEEE Trans Nucl Sci* 39(4):1099-1105, 1992.
24. Liang J, Jaszczak RJ, Coleman RE: Parameter estimation of finite mixtures using the EM algorithm and information criteria with application to medical image processing. *IEEE Trans Nucl Sci* 39(4):1126-1133, 1992.
25. Wang H, Jaszczak RJ, Coleman RE: Solid geometry based object model for Monte Carlo simulated emission and transmission tomographic imaging systems. *IEEE Trans Med Imaging* 11(3):361-372, 1992.
26. Johnson VE, Bowsher JE, Qian J, Jaszczak RJ: Segmentation and analysis of emission computed tomography images. *Neural and Stochastic Methods in Image and Signal Processing,* SPIE 1766:287-295, 1992.
27. Li J, Jaszczak RJ, Greer KL, Coleman RE, Cao Z, Tsui BMW: Direct cone beam SPECT reconstruction with camera tilt. *Phys Med Biol* 38:241-258, 1993.
28. Gilland DR, Tsui BW, Metz CE, Jaszczak RJ, Perry R: An evaluation of maximum likelihood EM reconstruction for SPECT by ROC analysis. *J Nucl Med* 33:451-457, 1992.
29. Leichner PK, Koral KF, Jaszczak RJ, Green AJ, Chen G, Roeske JC: An overview of imaging techniques and physical aspects of treatment planning in radioimmunotherapy. *Med Phys* 20(2):569-577, 1993.
30. Schold SC, Zalutsky MR, Coleman RE, Glantz MJ, Friedman AH, Jaszczak RJ, Bigner SH, Bigner DD: Distribution and dosimetry of 123-I labeled monoclonal antibody 81C6 in patients with anaplastic glioma. *Investigative Radiology* 28(6):488-496, 1993.
31. Li J, Jaszczak RJ, Turkington TG, Greer KL, Coleman RE: SPECT reconstruction of combined cone beam and parallel hole collimation with experimental data. *IEEE Trans Nucl Sci* 40(3):300-306, 1993.
32. Li J, Jaszczak RJ, Wang H, Greer KL, Coleman RE: Determination of both mechanical and electronic shifts in cone beam SPECT. *Phys Med Biol* 38:743-754, 1993.
33. Marks LB, Spencer DP, Bentel GC, Ray SK, Sherouse GW, Sontag MR, Coleman RE, Jaszczak RJ, Turkington TG, Tapson V, Prosnitz LR. The utility of SPECT lung perfusion scans in minimizing and assessing the physiologic consequences of thoracic irradiation. *Int J Radiation Oncology Biol Phys* 26:659-668, 1993.
34. Wang H, Jaszczak RJ, Coleman RE: A new composite model of objects for Monte Carlo simulation of radiological imaging. *Phys Med Biol* 38:1235-1262, 1993.
35. Wang H, Jaszczak RJ, Gilland DR, Greer KL, Coleman RE: Solid geometry based modeling of non-uniform attenuation and Compton scattering in objects for SPECT imaging systems. *IEEE Trans Nucl Sci* 40(4):1305-1312, 1993.
36. Smith MF, Floyd CE, Jaszczak RJ: A vectorized Monte Carlo code for modeling photon transport in SPECT: *Med Phys* 20(4):1121-1127, 1993.
37. Zeng GL, Gullberg GT, Jaszczak RJ, Li J: Fan-beam reconstruction algorithm for a spatially varying focal length collimator. *IEEE Trans Med Imaging* 12(3): 575-582, 1993.
38. Lowe VJ, Greer KL, Hanson MW, Jaszczak RJ, Coleman RE: Cardiac phantom evaluation of simultaneously acquired dual-isotope rest Thallium-201/Stress Technetium-99m SPECT images. *J Nucl Med* 34:1998-2006, 1993.
39. Li J, Jaszczak RJ, Turkington TG, Metz CE, Gilland DR, Greer KL, Coleman RE: An evaluation of lesion detectability with cone-beam, fan-beam and parallel-beam collimation in SPECT by continuous ROC study. *J Nucl Med* 35:135-140, 1994.
40. Li J, Jaszczak RJ, Greer KL, Coleman RE: A filtered backprojection algorithm for pinhole SPECT with a displaced center of rotation. *Phys Med Biol* 39:165-176, 1994.
41. Li J, Jaszczak RJ, Wang H, Gullberg GT, Greer KL, Coleman RE: A cone beam SPECT reconstruction algorithm with a displaced center of rotation. *Med Phys* 21:145-152, 1994.
42. Li J, Jaszczak RJ, Greer KL, Coleman RE: Implementation of an accelerated iterative algorithm for cone-beam SPECT. *Phys Med Biol* 39:643-653, 1994.

43. Smith MF, Jaszczak RJ: Generalized dual-energy-window scatter compensation in spatially varying media for SPECT. *Phys Med Biol* 39:531-546, 1994.
44. Smith MF, Jaszczak RJ: Simultaneously constraining SPECT activity estimates with primary and secondary energy window projection data. *IEEE Trans Med Imag* 13(2):329-337, 1994.
45. Wang H, Jaszczak RJ, Coleman RE: Information analysis for 3D SPECT imaging of radionuclide distributions in attenuating objects. *IEEE Trans Nucl Sci* 41(4):1612-1619, 1994.
46. Jang SB, Jaszczak RJ, Li J, Debatin JF, Nadel SN, Evans AJ, Greer KL, Coleman RE: Cardiac ejection fraction and volume measurements using dynamic cardiac phantoms and radionuclide imaging. *IEEE Trans Nucl Sci* 41(6):2845-2849, 1994.
47. Luo J, Ljungberg M, Koral KF, Floyd CE, Jaszczak RJ: A Monte-Carlo investigation of dual-energy-window scatter correction for volume-of-interest quantification in Tc-99m SPECT. *Phys Med Biol*, 40:181-199, 1995.
48. Li J, Jaszczak RJ, Greer KL, Gilland DR, Coleman RE: Evaluation of SPECT quantification of radiopharmaceutical distribution in canine myocardium. *J Nucl Med*, 36(2):278-286, 1995.
49. Li J, Jaszczak RJ, Wang H, Coleman RE: A filtered backprojection algorithm for fan-beam SPECT which corrects for patient motion. *Phys Med Biol*, 40:283-294, 1995.
50. Li J, Jaszczak RJ, Coleman RE: Maximum likelihood reconstruction for converging beam SPECT with a displaced center of rotation. *IEEE Trans Nucl Sci*, in press, 1995.
51. Wang H, Jaszczak RJ, Greer KL, Coleman RE: Monte Carlo modeling of cone beam collimation for detected Compton Scatter events. *IEEE Trans Nucl Sci*, in press, 1995.
52. Li J, Jaszczak RJ, Coleman RE: Maximum likelihood reconstruction for pinhole SPECT with a displaced center of rotation. *IEEE Trans Med Imag*, in press, 1995.
53. Kadrmas DJ, Jaszczak RJ, McCormick JW, Coleman RE: Truncation artifact suppression in transmission CT for improved SPECT attenuation compensation. *Phys Med Biol*, in press, 1995.
54. Marks LB, Prosnitz LR, Coleman RE, Jaszczak RJ: The role of function lung imaging in radiation therapy planning: The functional DVH. *Intl J of Rad Onc Biol Phys*, in press, 1995.
55. Li J, Jaszczak RJ, Coleman RE: A filtered backprojection algorithm for axial head motion correction in fan beam SPECT. *Phys Med Biol*, submitted, 1995.
56. Jang S, Jaszczak RJ, Greer KL, Coleman RE: Evaluation of ejection fraction measurements in gated cardiac imaging using dynamic cardiac phantoms. *IEEE Trans Nucl Sci*, in press, 1995
57. Li J, Jaszczak RJ, van Mullekom A, Scarfone C, Greer KL, Coleman ER: Halfcone beam collimation for triple-camera SPECT systems. *J Nucl Med*, submitted, April 1995.
58. Wang H, Jaszczak RJ, Coleman RE: Solid angles of elliptically circular acceptance cones of a fan beam collimator for SPECT imaging systems. *Review of Scientific Instruments*, submitted, 1995.
59. Johnson VE, Bowsher JE, Jaszczak RJ, Turkington TG. Analysis and reconstruction of medical images using prior information. In: *Case Studies in Applied Bayesian Statistics II with Discussion* (Springer-Verlag), in press, 1995.
60. Li J, Jaszczak RJ, Coleman RE: Axial head motion correction in fan-beam SPECT. 1995 International Meeting on Fully 3D Image Reconstruction in Radiology and Nuclear Medicine, France, June 1995, abstract accepted (manuscript in preparation), 1995.

1.3.4. Book Chapters and Conference Proceedings <u>supported fully or mainly</u> by this grant since the application was last submitted for competitive renewal (3/92 - 5/95)

61. Turkington TG, Gilland DR, Greer KL, Smith MF, Jaszczak RJ, Coleman RE: A direct measurement of skull attenuation for quantitative SPECT. In: *Conference Record of the 1992 IEEE Nuclear Science Symposium and Medical Imaging Conference* (Orlando, FL, 1992), pp. 1053-1055, 1993.
62. Jaszczak RJ, Gilland DR, Greer KL: Fast transmission CT for determining attenuation maps using a collimated, shuttered line source and fan beam collimation. In: *Conference Record of the 1992 IEEE Nuclear Science Symposium and Medical Imaging Conference* (Orlando, FL, 1992), pp. 991-993, 1993.
63. Smith MF, Gilland DR, Jaszczak RJ, Coleman RE: Estimation of tumor activities from simulated I-123 SPECT studies. *Conference Record of the 1994 IEEE Nuclear Science Symposium and Medical Imaging Conference* (Norfolk, Virginia, November 1994), 1920-1924, 1995.
64. Gilland DR, Jaszczak RJ, Greer KL, Coleman RE: Measured accuracy and precision in quantitative SPECT imaging with Iodine-123. *Conference Record of the 1994 IEEE Nuclear Science Symposium and Medical Imaging Conference* (Norfolk, Virginia, November 1994), pp. 1182-1186, 1995.
65. Wang H, Jaszczak RJ, Kadrmas D, Li J, McCormick JW, Coleman RE: Experimental evaluation of a Tellurium-123m transmission source to determine attenuation maps for SPECT. *Conference Record*

of the 1994 IEEE Nuclear Science Symposium and Medical Imaging Conference (Norfolk, Virginia, November 1994), 1553-1557, 1995.

66. Johnson EL, Jaszczak RJ, Wang H, Li J, Coleman RE: Pinhole SPECT for imaging In-111. *Conference Record of the 1994 IEEE Nuclear Science Symposium and Medical Imaging Conference* (Norfolk, Virginia, November 1994), 1888-1892, 1995.
67. Wang H, Jaszczak RJ, Johnson EL, Coleman RE: Monte Carlo modeling of penetration effect for iodine-131 pinhole imaging. *IEEE Nuclear Science Symposium and Medical Imaging Conference* (San Francisco, October 1995), abstract submitted (manuscript in preparation), 1995.
68. Smith MF, Jaszczak RJ, Wang H, Li J: Application of lead and tungsten pinhole inserts to I-131 SPECT tumor imaging: a Monte Carlo investigation. *Conference Record of the 1995 IEEE Nuclear Science Symposium and Medical Imaging Conference* (San Francisco, October 1995), abstract submitted (manuscript in preparation), 1995.
69. Gilland DR, Johnson EL, Turkington TG, Coleman RE, Jaszczak RJ: SPECT imaging of iodine-131 distribution in the head. *Conference Record of the 1995 IEEE Nuclear Science Symposium and Medical Imaging Conference* (San Francisco, October 1995), abstract submitted (manuscript in preparation), 1995.

1.3.5. Book Chapters and Conference Proceedings <u>supported in part</u> by this grant since the application was last submitted for competitive renewal (3/92 - 5/95)

70. Li J, Jaszczak RJ, Wang H, Greer KL, Coleman RE: Determination of both mechanical and electronic shifts in cone beam SPECT. In: *Conference Record of the 1992 IEEE Nuclear Science Symposium and Medical Imaging Conference* (Orlando, FL, 1992), pp. 1062-1064, 1993.
71. Wang H, Jaszczak RJ, Hawman EG, Greer KL, Coleman RE: Forced detection for astigmatic collimation based on circular acceptance cone approximation. In: *Conference Record of the 1992 IEEE Nuclear Science Symposium and Medical Imaging Conference* (Orlando, FL, 1992), pp. 1092-1094, 1993.
72. Wang H, Greer KL, Jaszczak RJ, Coleman RE: Monte Carlo modeling of cone beam collimation with scattering in objects. In: *Conference Record of the 1992 IEEE Nuclear Science Symposium and Medical Imaging Conference* (Orlando, FL, 1992), pp. 1224-1226, 1993.
73. Smith MF, Jaszczak RJ, Coleman RE: Simultaneously constraining SPECT activity estimates with primary and secondary energy window projection data. *Conference Record of the 1992 IEEE Nuclear Science Symposium and Medical Imaging Conference* (Orlando, FL, 1992), pp. 1175-1177, 1993.
74. Li J, Jaszczak RJ, Coleman RE: Maximum likelihood reconstruction for converging beam SPECT with a displaced center-of-rotation. *Conference Record of the 1993 IEEE Nuclear Science Symposium and Medical Imaging Conference* (San Francisco, 1993), pp. 1769-1773, 1994.
75. Wang H, Jaszczak RJ, Coleman RE: Information analysis for 3D SPECT imaging of radionuclide distributions in attenuating objects. *Conference Record of the 1993 IEEE Nuclear Science Symposium and Medical Imaging Conference* (San Francisco, 1993), pp. 1386-1390, 1994.
76. Bowsher JE, Johnson VE, Turkington TG, Floyd CE, Jaszczak RJ, Coleman RE: Improved lesion detection and quantification in emission tomography using anatomical and physiological prior information. *Conference Record of the 1993 IEEE Nuclear Science Symposium and Medical Imaging Conference* (San Francisco, 1993), pp. 1907-1911, 1994.
77. Jang S, Jaszczak RJ, Li J, Debatin JF, Nadel SN, Evans AJ, Greer KL, Coleman RE: Study of cardiac ejection fraction and volume measurements using a dynamic cardiac phantom and SPECT. *Conference Record of the 1993 IEEE Nuclear Science Symposium and Medical Imaging Conference* (San Francisco, 1993), pp. 1581-1585, 1994.
78. Jaszczak RJ, Tsui BMW: Single photon emission computed tomography. In: *Principles of Nuclear Medicine*, Eds. HN Wagner and Z Szabo (W.B. Saunders, Philadelphia, 1994), in press, 1995.
79. Jaszczak RJ, Hoffman EJ: Scatter and attenuation. In: *Principles of Nuclear Medicine*, eds. HN Wagner and Z Szabo (W.B. Saunders, Philadelphia, 1994), in press, 1995.
80. Kadrmas DJ, Jaszczak RJ, Coleman RE: FB-TCT truncation suppression by combining two shifted scans with extrapolation techniques. *Conference Record of the 1994 IEEE Nuclear Science Symposium and Medical Imaging Conference* (Norfolk, Virginia, November 1994), 1247-1250, 1995.
81. Li J, Jaszczak RJ, Greer KL, Coleman RE: Quantitative small field-of-view pinhole SPECT imaging: Initial evaluation. *Conference Record of the 1994 IEEE Nuclear Science Symposium and Medical Imaging Conference* (Norfolk, Virginia, November 1994), 1187-1191, 1995.
82. Jang S, Jaszczak RJ, Greer KL, Coleman RE: Evaluation of ejection fraction measurements in gated cardiac imaging using a dynamic cardiac phantom. *Conference Record of the 1994 IEEE Nuclear*

Science Symposium and Medical Imaging Conference (Norfolk, Virginia, November 1994), 1735-1738, 1995

83. Jang S, Jaszczak RJ, Li J, Lowe VJ, Greer KL, Coleman RE: Scatter corrections for simultaneously acquired dual-isotope SPECT imaging using three windows. *Conference Record of the 1994 IEEE Nuclear Science Symposium and Medical Imaging Conference* (Norfolk, Virginia, November 1994), 1493-1497, 1995.
84. Wang H, Jaszczak RJ, Coleman RE: A filtered backprojection algorithm for astigmatic SPECT reconstruction. *Conference Record of the 1994 IEEE Medical Imaging Conference* (Norfolk, Virginia, November 1994), pp. 1925-1929, 1995.
85. Friedman AH, Drayer BP, Jaszczak RJ: Single photon tomography. In *Neurosurgery*, Eds.: R.H. Wilkins and S.S. Rengachary (McGraw-Hill, New York, 1994), in press, 1995.
86. Wang H, Jaszczak RJ, Johnson EL, Coleman RE: Monte Carlo modeling of penetration effect for iodine-131 pinhole imaging. *Conference Record of the 1995 IEEE Nuclear Science Symposium and Medical Imaging Conference* (San Francisco, October 1995), abstract submitted (manuscript in preparation), 1995.
87. Wang H, Jaszczak RJ, Coleman RE: Determination of collimator and acquisition parameters for astigmatic SPECT imaging. *Conference Record of the 1995 IEEE Nuclear Science Symposium and Medical Imaging Conference* (San Francisco, October 1995), abstract submitted (manuscript in preparation), 1995.
88. Li J, Jaszczak RJ, Greer KL, Coleman RE: Experimental evaluation of a super-high resolution, five-pinhole SPECT system. *Conference Record of the 1995 IEEE Nuclear Science Symposium and Medical Imaging Conference* (San Francisco, October 1995), abstract submitted (manuscript in preparation), 1995.
89. McCormick JW, Jaszczak RJ, Gilland DR, Coleman RE: The effect of truncation reduction in fan beam transmission for non-uniform attenuation correction of cardiac SPECT. *Conference Record of the 1995 IEEE Nuclear Science Symposium and Medical Imaging Conference* (San Francisco, October 1995), abstract submitted (manuscript in preparation), 1995.
90. Bowsher JE, Johnson VE, Turkington TG, Jaszczak RJ, Coleman RE: Effects of physical modeling on Bayesian SPECT reconstruction into regions. *Conference Record of the 1995 IEEE Nuclear Science Symposium and Medical Imaging Conference* (San Francisco, October 1995) abstract submitted (manuscript in preparation), 1995.
91. Johnson V, Higdon DM, Gilland D, Turkington T, Jaszczak RJ, Bowsher J: Bayesian Estimation of Gibbs hyperparameters in emission computed tomography data. *Conference Record of the 1995 IEEE Nuclear Science Symposium and Medical Imaging Conference* (San Francisco, October 1995) abstract submitted (manuscript in preparation), 1995.

1.3.6. Abstracts supported fully, mainly, or partially by this grant since the application was last submitted for competitive renewal (3/92-5/95)

During the past project period, this grant has supported fully, mainly, or partially 44 abstracts.